Computers & Geosciences 62 (2014) 227–240

Contents lists available at ScienceDirect

Computers & Geosciences

journal homepage: www.elsevier.com/locate/cageo

XMapTools: A MATLAB©-based program for electron microprobe X-ray image processing and geothermobarometry

Pierre Lanari [a,b,*], Olivier Vidal [b], Vincent De Andrade [c], Benoît Dubacq [d,e,f], Eric Lewin [b], Eugene G. Grosch [g], Stéphane Schwartz [b]

[a] Institute of Geological Sciences, University of Bern, Baltzestrasse 1+3, CH-3012 Bern, Switzerland
[b] ISTerre, Universite de Grenoble I, CNRS, 1381 rue de laPiscine, 38041 Grenoble, France
[c] NSLS II, Brookhaven National Laboratory, SRX beamline, Bldg 817 Renaissance Road, Upton, NY 11973, USA
[d] Department of Earth Sciences, University of Cambridge, Downing Street, Cambridge CB2 3EQ, UK
[e] UPMC University of Paris 06, ISTEP, UMR 7193; F-75005 Paris, France
[f] CNRS, ISTEP, UMR 7193; F-75005 Paris, France
[g] Department of Earth Science and Centre for Geobiology, University of Bergen, Allegaten 41, N-5007, Bergen, Norway

ARTICLE INFO

Article history:
Received 4 January 2013
Received in revised form
23 August 2013
Accepted 27 August 2013
Available online 7 September 2013

Keywords:
XMapTools program
X-ray chemical imaging
Quantitative micro-mapping
PT-maps

ABSTRACT

XMapTools is a *MATLAB*©-based graphical user interface program for electron microprobe X-ray image processing, which can be used to estimate the pressure–temperature conditions of crystallization of minerals in metamorphic rocks. This program (available online at http://www.xmaptools.com) provides a method to standardize raw electron microprobe data and includes functions to calculate the oxide weight percent compositions for various minerals. A set of external functions is provided to calculate structural formulae from the standardized analyses as well as to estimate pressure–temperature conditions of crystallization, using empirical and semi-empirical thermobarometers from the literature. Two graphical user interface modules, *Chem2D* and *Triplot3D*, are used to plot mineral compositions into binary and ternary diagrams. As an example, the software is used to study a high-pressure Himalayan eclogite sample from the Stak massif in Pakistan. The high-pressure paragenesis consisting of omphacite and garnet has been retrogressed to a symplectitic assemblage of amphibole, plagioclase and clinopyroxene. Mineral compositions corresponding to ~165,000 analyses yield estimates for the eclogitic pressure–temperature retrograde path from 25 kbar to 9 kbar. Corresponding pressure–temperature maps were plotted and used to interpret the link between the equilibrium conditions of crystallization and the symplectitic microstructures. This example illustrates the usefulness of *XMapTools* for studying variations of the chemical composition of minerals and for retrieving information on metamorphic conditions on a microscale, towards computation of continuous pressure–temperature-and relative time path in zoned metamorphic minerals not affected by post-crystallization diffusion.

1. Introduction

Our understanding of the geodynamics and processes in orogens, subduction zones and the lower crust relies on estimations of the pressure–temperature (*P*–*T*) conditions of crystallization of mineral assemblages. Deriving reliable pressure and temperature information from a rock is critical to our knowledge of the thermal structure of the crust, whose variations can be recorded through time within individual samples via consecutive partial re-equilibration events. Thermobarometric tools such as multi-equilibrium thermobarometry (e.g. Berman, 1991), pseudosections (e.g. Holland and Powell, 1998, 2011) and empirical thermometers (e.g. Cathelineau and Nieva, 1985) provide these estimates from the nature and composition of minerals, even for high-variance assemblages (Vidal and Parra, 2000). To shed light on the recrystallization history of metamorphic rocks, chemical compositions of the minerals are required. This is commonly achieved using point mode analyses obtained with an electron probe microanalyser (EPMA). The use of X-ray images allows to identify the relationships between microstructures, variations of composition and variations of *P*–*T* conditions of crystallization (e.g. Vidal et al., 2006). Since the first X-ray "dot maps" compositional image (Cosslett and Duncumb, 1956), this technique has been developed (see Friel and Lyman, 2006 for a review) using both energy-dispersive and wavelength dispersive X-ray spectrometers (EDS and WDS). For instance, previous work has used X-ray images for classification and modal analysis (Launeau et al., 1994;

* Corresponding author at: Institute of Geological Sciences, University of Bern, Baltzestrasse 1+3, CH-3012 Bern, Switzerland. Tel.: +41 31 631 87 61; fax: +41 31 631 48 43.
E-mail addresses: pierre.lanari@geo.unibe.ch, pierre.lanari@gmail.com (P. Lanari).

0098-3004/$ - see front matter © 2013 Elsevier Ltd. All rights reserved.
http://dx.doi.org/10.1016/j.cageo.2013.08.010

Table 1
List of solid-solution models and associated end-members included in *XMapTools*.

Group	Mineral*	End-members**	References
Chain silicates	Amphibole (23)	*glaucophane* (*gl*) *tremolite* (*tr*) *Fe-tremolite* (*ftr*) *tschermakite* (*ts*) *pargasite* (*parg*) *cummingtonite* (*cum*)	Holland and Blundy, 1994, Dale et al. (2000, 2005), Spear (1995)
	Clinopyroxene (6)	*jadeite* (*jd*) *diopside* (*di*) *hedenbergite* (*hed*) Ca-*tschermak* (*cats*) *acmite* (*acm*)	Spear (1995); Warren and Waters (2006)
	Orthopyroxene (6)	*enstatite* (*en*) *ferrosilite* (*fs*) *Mg-tschermak* (*mgts*)	Holland and Powell (1998)
	Chloritoid (6)	*Fe-chloritoid* (*fctd*) *Mg-chloritoid* (*mctd*) *Mn-chloritoid* (*mnctd*)	Vidal et al. (1999)
	Staurolite (48)	*Fe-staurolite* (*fst*) *Mg-staurolite* (*mst*) *Mn-staurolite* (*mnst*)	Holland and Powell, (1998)
	Epidote (12.5)	*zoizite* (*zo*) *epidote* (*ep*) *Fe-epidote* (*fep*)	Holland and Powell, (1998)
	Cordierite (18)	*cordierite* (*crd*) *Fe-cordierite* (*fcrd*) *Mn-cordierite* (*mncrd*)	Holland and Powell, (1998)
Ortho- & ring silicates	Garnet (12)	*almandine* (*alm*) *pyrope* (*pyr*) *spessartine* (*spe*) *grossular* (*gro*)	Spear (1995)
	Olivine (4)	*forsterite* *fayalite*	Spear (1995)
Phylosilicates	Chlorite (14)	*amesite* (*ames*) *Fe-amesite* (*fames*) *daphnite* (*daph*) *sudoite* (*sud*) *chlorite-Mg* (*afchl*) *chlorite-Fe* (*fafchl*)	Holland et al. (1998); Vidal et al. (2001, 2005, 2006)
	Micas (11)	*celadonite* (*cel*) *Fe-celadonite* (*fcel*) *muscovite* (*mus*) *paragonite* (*par*) *margarite* (*marg*) *phlogopite* (*phl*) *Fe-phlogopite* (*fphl*) *pyrophylite* (*prl*)	Coggon and Holland (2002); Parra et al. (2002); Dubacq et al. (2010)
Framework silicates	Feldspar (8)	*albite* (*ab*) *anortite* (*an*) *microcline* (*mic*)	Spear (1995)

* Oxygen basis
** Abbreviation

Bonnet, 1998; Cossio et al., 2002; Prêt et al., 2010; Martin et al., 2013) and to reconstruct *P–T* paths (Kohn and Spear, 2000; De Andrade et al., 2006; Muñoz et al., 2006; Vidal et al., 2006; Yamato et al., 2007; Ganne et al., 2012; Fiannacca et al., 2012; Lanari et al., 2012; Plunder et al., 2012; Pourteau et al., 2013; Lanari et al., 2013). Quantitative electron microprobe analyses require an analytical standardization of the number of collected photons (X-ray intensity). The acquisition time for standardized point analysis for eight major elements (e.g. Si, Al, Mn, Mg, Fe, Na, Ca, K) under classical conditions (typically 10 nA, 15 keV, 40 s) averages around two minutes. This approach is therefore difficult to apply to chemical mapping, where samples are typically heterogeneous on a ~10 μm scale and maps typically contain about 150,000 pixels, that would correspond to ~200 days of measurements. X-ray maps for quantitative mapping can be obtained within a reasonable time frame by using a higher current intensity and a lower counting time (100 nA, 15 KeV, 100–300 ms, see De Andrade et al., 2006). In order to transform the X-ray intensities into calibrated weight percentages, Clarke et al. (2001) used a Bence–Albee approach (Bence and Albee, 1968), which has been later implemented in the program *XRMapAnal* (Tinkham and Ghent, 2005). However, the precision of this standardization procedure is subject to caution, because it can result in unreliable compositions for some geologically important phases (e.g. quartz, muscovite, plagioclase and garnet, compositions listed in the Table 3 of Tinkham and Ghent, 2005). De Andrade et al. (2006) showed that standardization of X-ray intensities using point analyses as internal standards (Castaing, 1951) provides more reliable results.

In the present contribution, we present a *MATLAB*©-based Graphical User Interface (GUI) program named *XMapTools* that can be used to: (1) classify mineral phases in the sample, (2) convert X-ray intensities into calibrated weight percentages using Castaing's approach, (3) calculate the structural formulae of the

Table 2
List of exchange reaction calibrations included in *XMapTools*.

Method	Calibrations
Amphibole–Plagioclase	Blundy and Holland (1990), and Holland and Blundy (1994)
Chlorite–Chloritoid	Vidal et al. (1999)
Garnet–Biotite	Thompson (1976), Goldman and Albee (1977), and Holdaway and Lee (1977)
Garnet–Muscovite	Green and Hellman (1982), and Krogh and Råheim (1978)
Garnet–Chlorite	Dickenson and Hewitt (1986), and Grambling (1990)
Garnet–Amphibole	Ravna (2000b), Perchuk et al. (1985), and Graham and Powell (1984)
Garnet–Cpx	Ravna (2000a), Ai (1994), Sengupta et al. (1989), Pattison and Newton (1989), Krogh (1988), Powell (1985), Dahl (1980), Ganguly (1979), Ellis and Green (1979), Mori and Green (1978), Råheim and Green (1974), and Mysen and Heier (1972)

Table 3
List of empirical thermometers, barometers and multi-equilibrium functions implemented in XMapTools.

Mineral	Thermometers	Barometers	Multi-equilibrium
Amphibole	*T*; Holland and Blundy (1994)	*P*; Anderson and Smith (1995) *P*; Schmidt (1992) P; Johnson and Rutherford (1989) P_{min}; Johnson and Rutherford (1989) P_{max}; Johnson and Rutherford (1989) *P*; Hollister et al. (1987) *P*; Hammarstrom and Zen (1986)	**Amphibole**+**plagioclase*** *P* from Schmidt (1992) and *T* from Holland and Blundy (1994) **Amphibole**+**plagioclase***+**quartz*** *P* from Schmidt (1992) and *T* from Holland and Blundy (1994)
Chlorite	*T*; Inoue et al. (2009) *T*; Zang and Fyfe (1995) *T*; Jowett (1991) *T*; Hillier and Velde (1991) *T*; Cathelineau (1988) *T*; Kranidiotis and MacLean (1987); *T*; Cathelineau and Nieva (1985)		
Clinopyroxene		*P*; Waters (2002, 2003)	**Cpx**+**garnet***+**phengite*** *P* from garnet–omphacite–phengites barometer of Waters and Martin (1993) and Waters (1996) and *T* from garnet–omphacite thermometer of Ravna (2000a) or Ellis and Green (1979) **Cpx**+**amphibole***+**plagio*** *T* from amphibole–plagioclase thermometer of Holland and Blundy (1994) and *P* for the cpx – plagioclase barometer of Waters (2002, 2003)
K-white mica		*P*; Massone and Schreyer (1987)	
Garnet	*T*; Creighton (2009) *T*; Kawasaki et al. (2011)		
Rutile	*T*; Zack et al. (2004)		

* Fixed composition

identified minerals, (4) plot minerals compositions using various chemical diagrams, and (5) calculate *P–T* conditions of equilibration using various empirical and semi-empirical thermobarometers. An example of application of the program to a retrogressed eclogite is presented below.

2. Description of the program

The *XMapTools* program (available at http://www.xmaptools.com) can be run with a *MATLAB*© version 7.5 release R2007b or later. It uses a graphical interface named *XMapTools.fig* (Fig. 1) built using the *MATLAB*© Graphical User Interface Development Environment (*GUIDE*) tool. Each of the GUI components dragged with the *GUIDE* is associated with a callback function in the program file *XMapTools.p*, corresponding to a content-obscured version (encrypted executable).

The program is structured into three parts: *Xray*, *Quanti* and *Results* (Fig. 2) corresponding to three different steps of the mapping process. The first step (*Xray* column in Fig. 2), starts by loading the map. From statistical analysis of their composition, pixels are grouped within mineral phases and possibly fractures or voids, and corresponding masks are created. The user then identifies the nature of the various groups. This steps ends with the standardization stage. In the second step, (*Quanti* column in Fig. 2), standardized maps are turned into maps of structural formulae and into *P–T* maps. The last step (*Results* column in Fig. 2), allows the user to produce binary and ternary chemical diagrams with the *Chem2D* and *TriPlot3D* modules. All the functions used in these different stages are detailed below.

2.1. Raw data treatment (Xray)

Two types of datasets can be uploaded into *XMapTools*, namely the raw X-ray data in photon counts per pixel (matrixes

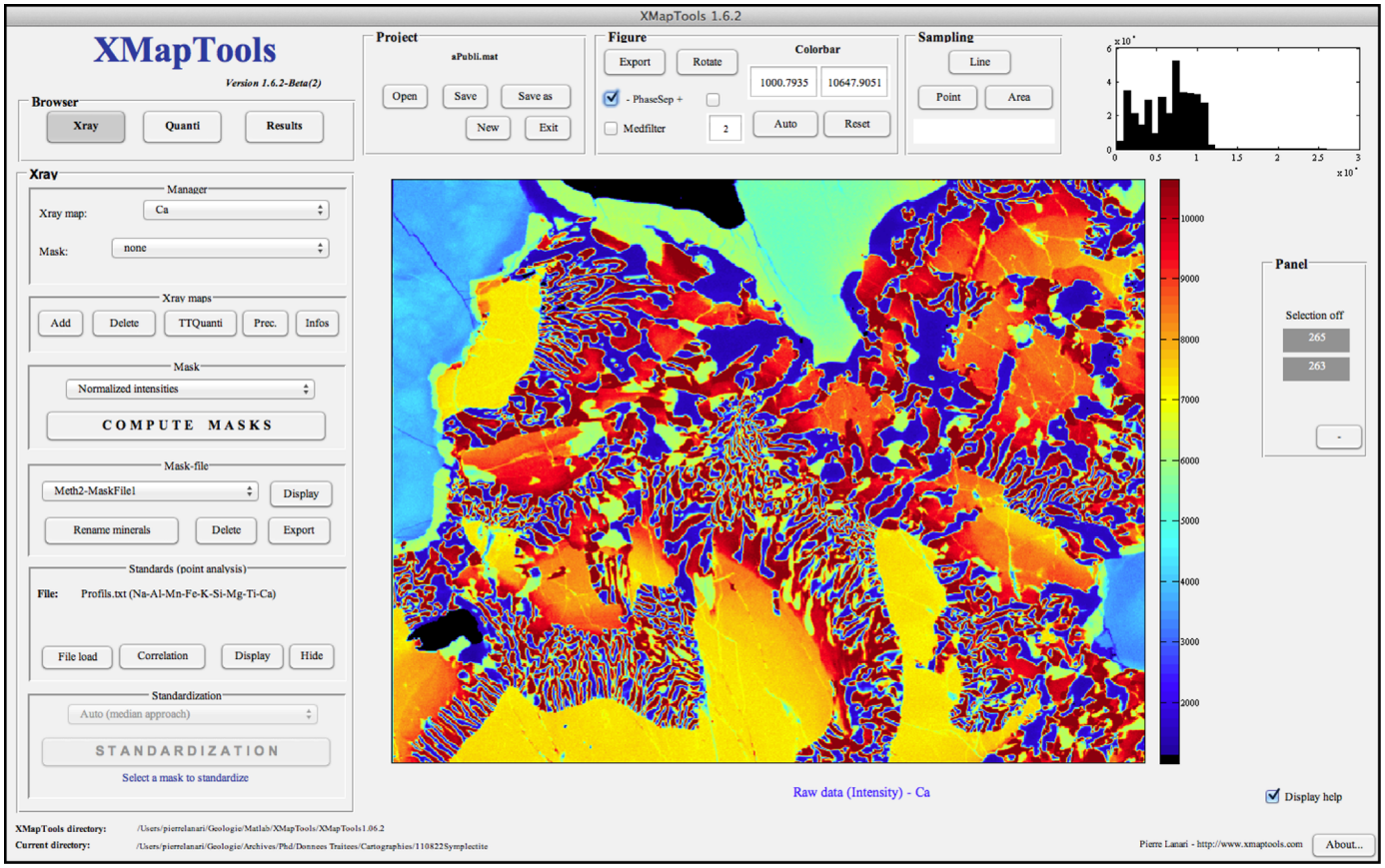

Fig. 1. *XMapTools* (v1.6.2) graphic user interface. The displayed image is the raw Al-content map of the sample 'Eclogite' (see text for details) unit: number of recorded counts.

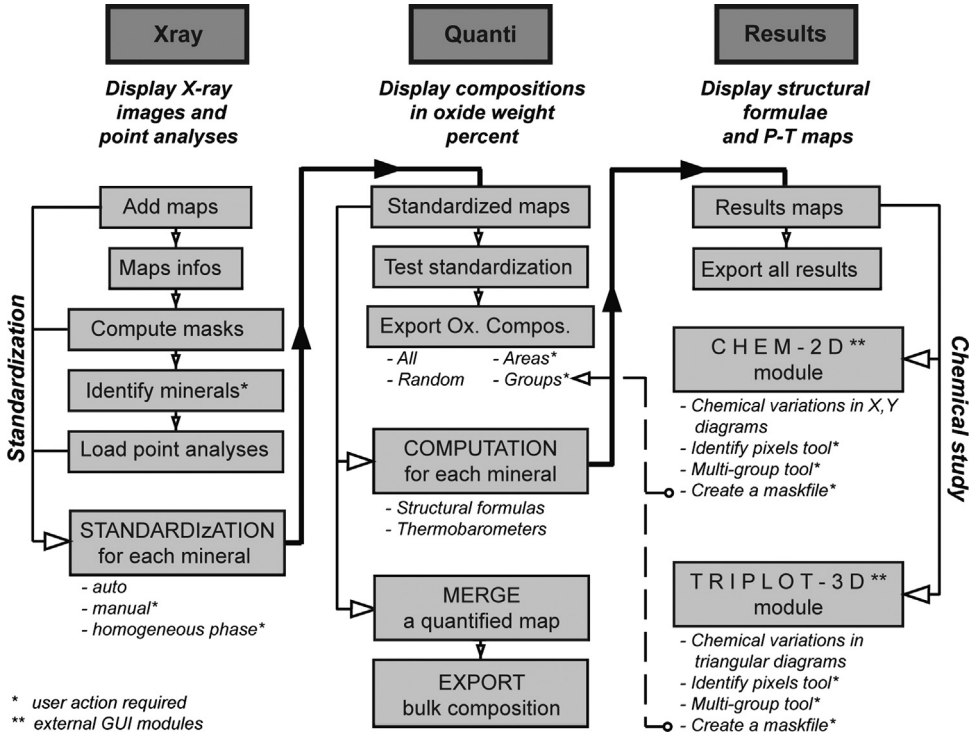

Fig. 2. *XMapTools* operating diagram, schematizing the structure of the program. All steps marked with a star require user action. Light arrows indicate the way forward, bold-arrows the transition between the different sub-programs (*Xray*, *Quanti*, *Results*, see text), and the dashed arrows the available feedback.

corresponding to the number of collected photons per analyzed element per pixel) and the point analyses used as internal standards.

With both *CAMECA*© and *JEOL*© EPMA, the raw data of chemical maps can be exported in *ASCII* format text files such as **.txt* file. Typically, one file is created for each measured element, and contains header lines reporting information about analytical conditions and coordinates of the selected area, followed by a matrix of X-ray intensity data (see Fig. A1 and Appendix 1). After removal of the header lines by the user, the loading function of *XMapTools* reads the input files and creates X-ray intensity images. This function includes dead-time correction, where the time interval after the arrival of a pulse during which the spectrometer is unresponsive to further pulses (Reed, 2005) is accounted for, and transforms the measured counting rates into true rates.

Point analyses, their coordinates and the map coordinates are the other required inputs to the standardization step. Usually, the point analyses are made along different transects at high angles to mineral grain boundaries to capture the total extent of the minerals heterogeneity. Experience has shown that a minimum of 20 point analyses encompassing most of the chemical heterogeneity of each mineral phases in the selected area of the sample is necessary to reach optimum precision. The standard loading function reads a series of point analyses. The locations of the point analyses must be carefully reported from stage coordinates corrected for mechanical backlash and are then projected on the map with the EMPA map coordinate system. The user can compare the X-ray intensities along the profiles measured by point analyses to those of the map, which is useful to detect problems of location of profiles on the map, for example due to drifting of the sample stage during analysis or to a projection problem. The point analyses showing outlying or unwanted compositions such as mixtures of fine minerals, inclusions, or grain boundaries must be deleted before the standardization.

2.1.1. Classification: mask creating function

This function creates masks corresponding to entities identified in the map (e.g. mineral, mineral boundaries, fractures), where each mask is a matrix of logical numbers indexed on the coordinates of the composition map: the value of 1 is attributed to the pixels belonging to a given mineral phase, and 0 to the other pixels. This function allocates each individual pixel to one of the minerals phases. The mask creating function uses the statistical analysis method *K-means* clustering to distribute the pixels into groups of similar compositions. *K-means* identifies clusters and allocates pixels to these clusters by minimization of the distance in compositional space between the pixels and the gravity center of each cluster (Saporta, 1990).

The user selects one pixel of each phase on the chemical map as needed by the mask creating function for initial guess. The compositions of these pixels are used as starting cluster centroids. In an iterative loop, each pixel is assigned to the nearest cluster and the centroids are recalculated until the sum of point-to-centroid distancesover all clusters is minimized (Seber, 1984; Spath, 1985). Two approaches are available in *XMapTools*: the 'normalized' and the 'classical' approaches. Both of them use a *K-means* clustering approach, but with different X-ray intensities inputs. In the 'normalized' function, X-ray intensities of each element are normalized to their mean values, with the result that all elements have the same weight and only the variances are compared. In contrast, the X-ray intensities of each element in the 'classical' method depend on the absolute concentration in each element. This 'classical' method is therefore more appropriate for elements present in high concentration. Different masks may be derived using both methods, depending on the magnitude of the differences between the compositions of the phases. An example is shown in Section 3.2. Other approaches for the classification of different mineral phases can be found in the *PetroMod* program (Cossio et al., 2002). Here the K-means algorithm was chosen for its straightforwardness and efficiency.

2.1.2. Standardization function

The analytical standardization consists in converting the measured X-ray intensities into oxide weight percent concentrations using standards (Reed, 2005). The standardization function performs this transformation for each mask where quantitative information is available from point analysis or using user-defined concentrations. The standardization of pixels requires calibration curves describing how X-ray intensities change with concentration (Castaing, 1951). One calibration curve is calculated for each element in each phase from the intensity versus concentration relations constrained with point analyses. The calibration curves for Si in the different phases of the studied sample are shown in Fig. 3. For each mineral, the calibration curve is a straight line between the origin (zero intensity and concentration) and the central point of the cluster of the point analyses.

The standardization can be performed using one of the three methods available in *XMapTools*. The first method 'Auto (median approach)' is fully automatic, and the cluster centroids are the median values separating the higher half from the lower half of the data. The 'Manual' approach allows the user to define the center of the clusters and therefore the calibration curve. The last method 'Manual (homogeneous phase)' is adapted to minerals assumed to be homogeneous such as might be the case for quartz. The calibration curve is then defined as the mean value of X-ray intensity for the selected mineral and the user enters the corresponding concentration, e.g. 100% for SiO_2 in the case of quartz.

2.2. Calculations from quantified data (Quanti)

Once the masks have been defined and element concentrations have been estimated, structural formulae may be calculated and equilibrium conditions derived using external functions (see below). Users can add new thermobarometry or structural formula functions. The file 'List-thermometers.txt' lists all information about these external functions (i.e. category, name, input and output variables) that are stored into the folder 'Functions'. All

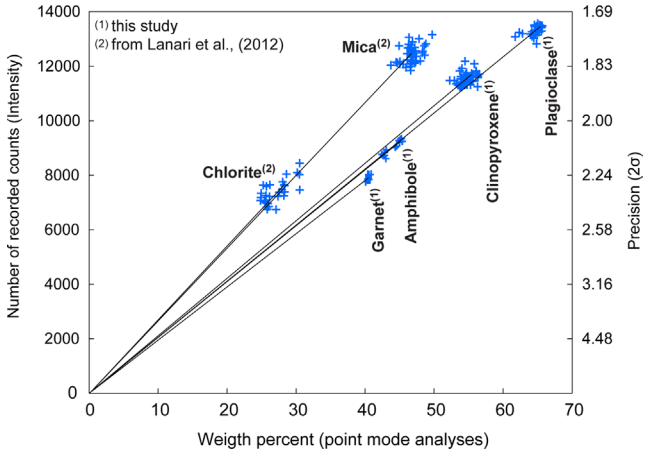

Fig. 3. Intensity recorded on the map versus oxide weight percent concentrations for Si in the studied sample. Blue crosses show point analyses, lines are regressed calibration curves obtained using the median approach described in text. The precision is given depending on the intensity (% at 2σ) following eq. 1 (see text).

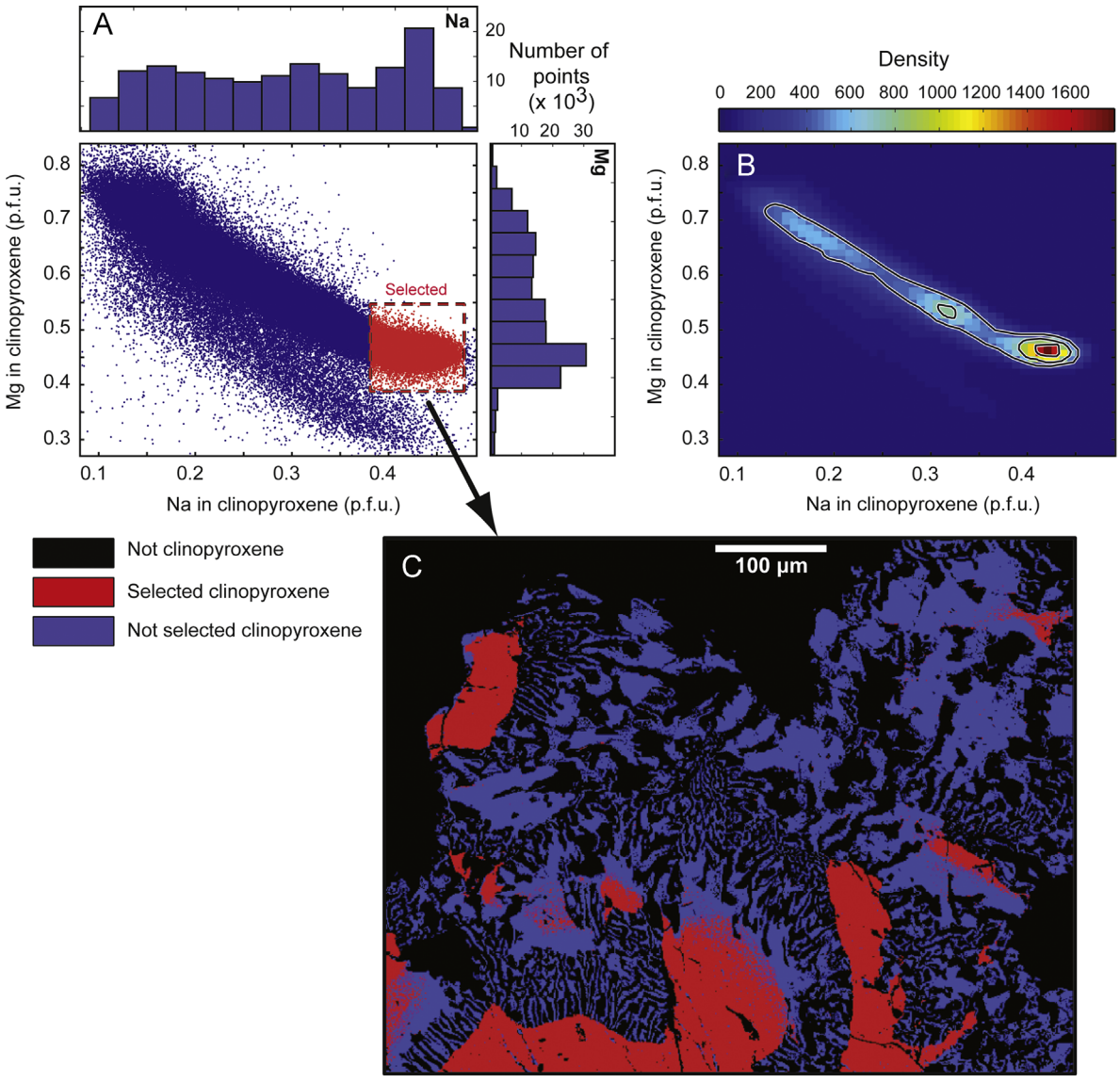

Fig. 4. Results from the *XMapTools Chem2D* module. (A) The clinopyroxene compositions are plotted in a binary diagram Na vs. Mg. Unit is per formula unit (p.f.u.). The pixels displayed in the map are colored in red. (B) Density map calculated from the binary diagram (see text for details). (C) Map of the analyzed area in which clinopyroxene pixels selected in A are in red and the unselected pixels in blue. Black pixels do not belong to the clinopyroxene mask. Selected Na-rich pixels correspond to 25% of the total clinopyroxene pixels. (For interpretation of the references to color in this figure legend, the reader is referred to the web version of this article.)

these functions are *MATLAB*© script m-files that can be read and edited.

2.2.1. *Structural formulae functions*

Several structural formulae and atom site allocations models from the literature are implemented in *XMapTools* (Table 1). A general function is also available to calculate a structural formula normalized to a given number of oxygen atoms. This additional function is used to compute the number of moles of elements per formula unit (p.f.u.) for each pixel assuming that the total sums up to 100%.

2.2.2. *Thermobarometry functions*

XMapTools includes a large selection of thermobarometry functions based on empirical and semi-empirical calibrations. These methods are distributed into two groups: exchange reactions for thermometry (Table 2) and thermobarometer functions (Table 3).

In exchange reactions, cations such as Fe^{2+} and Mg^{2+} are swapped between two minerals (e.g. Spear, 1995). *P–T* conditions of equilibrium may be derived from the cations partition between the two phases (e.g., Ravna, 2000a for garnet–clinopyroxene). *XMapTools* generates an image with the oxide weight percent compositions of the two minerals and allows the user to select pairs of pixels (spot mode) or pairs of groups of pixels (area mode).

In the spot mode, the selected compositions are used to estimate the equilibrium conditions. In the area mode, all the possible pairs of pixels are used to calculate an average equilibrium condition with associated uncertainty. This mode allows to propagate the effect of composition variation in any phase through the whole thermobarometer calculation.

For exchange reactions, *T* is usually estimated for a given pressure. If the minerals exhibit metamorphic zoning preserving paleo-equilibrium conditions, and if the zoning pattern is not due to post-crystallization diffusion, the variations of *T* conditions can be investigated using exchange reactions. A set of mineral pairs selected between the core and the rim of two minerals provides a

trend for the evolution of the temperature conditions. This approach is essentially the same as commonly used with point analyses.

The thermobarometry functions provide information on the *T* and/or *P* of mineral crystallization for each pixel of the map, which can be turned into *P*, *T*, or *P and T* maps. Both *P* and *T* conditions are derived from only one mineral composition (one pixel) with fixed variables such as other mineral composition, or *P* or *T*. Methods are listed in Table 3 in three groups: (1) thermometers, (2) barometers, and (3) thermobarometers where *P*–*T* conditions are derived from at least two reactions (one *T-dependent* and one *P-dependent*) within a given mineral assemblage. This is done using groups of pixel compositions and assuming equilibrium between the groups.

The use of thermobarometry functions should be restrained to cases where the relevant saturating assemblages are present in the studied sample. The functions implemented in *XMapTools* do not check the presence of such assemblages because some minerals may be outside the mapped area. It is then the responsibility of the user to decide whether the functions can be applied to the studied sample.

2.3. Chemical plots (Results)

The mineral compositions or end-member proportions can be plotted as maps or into chemical diagrams such as binary diagrams (Fig. 4a) using the *Chem2D* module, or ternary diagrams (Fig. 5a) using the *Triplot3D* module. Both modules have a graphical interface in which the user can select the plotted variables and manage the diagram axes. A density plot function is also available to contour the analyzed variables for density, which is useful when a large number of points is plotted as is the case when working with maps (see examples in Figs. 4 and 5b). This function displays a density map using the mineral composition data and grid spacing defined by the user for density counting. The unit of the output of the density map is a number of analyses per surface unit of the grid on the graph, which has the dimension of the *x* axis multiplied to the *y* axis.

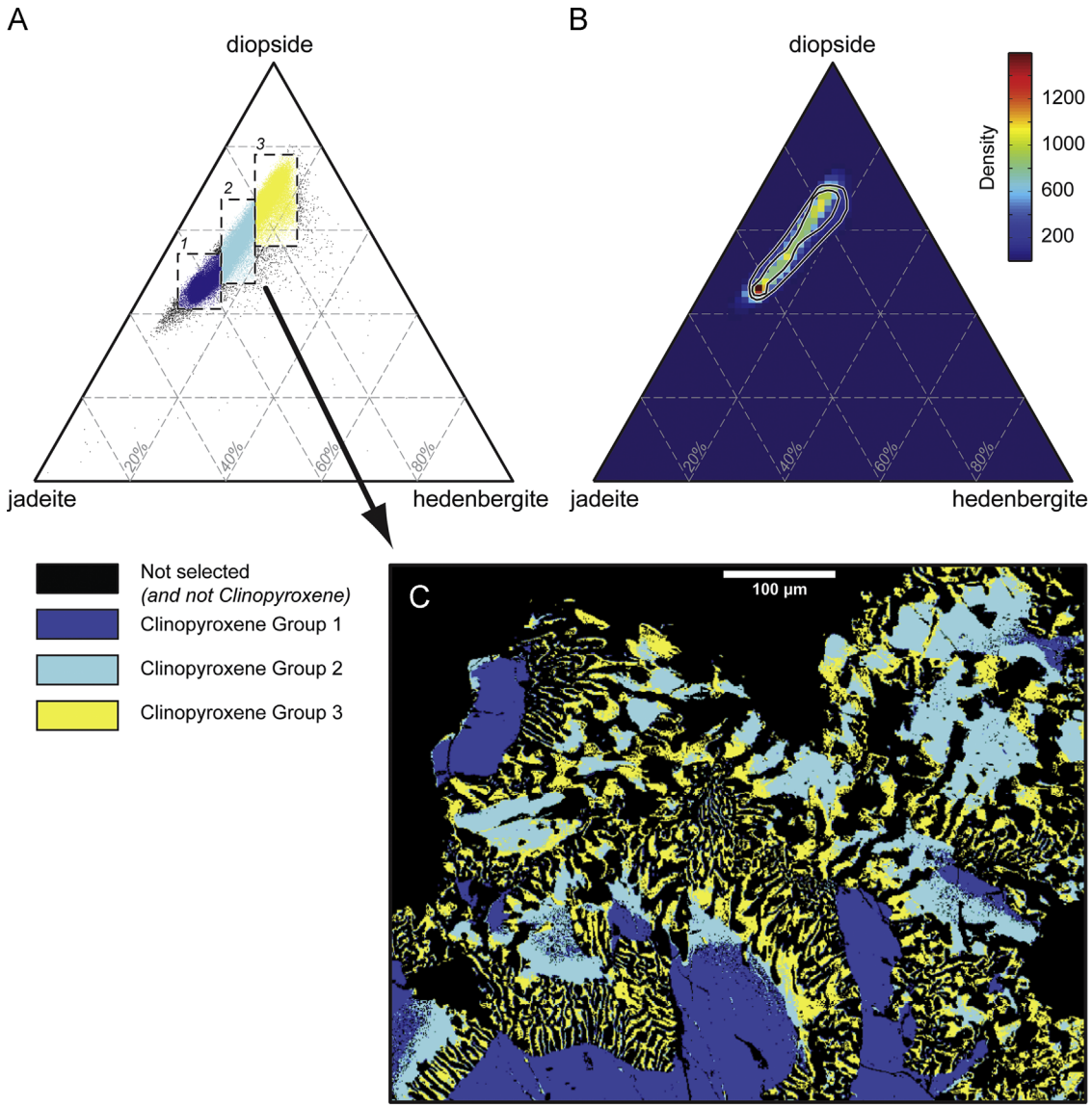

Fig. 5. Results from the *XMapTools TriPlot3D* module. (A) Clinopyroxene compositions plotted in a ternary diagram jadeite-diopside-hedenbergite. Unit is the end-member proportion. The selected pixel groups displayed into a map in C are colored according to their group (blue: group 1, cyan: group 2, yellow: group 3). (B) Density map calculated from the ternary diagram. (C) Map of the analyzed area, in which the selected groups of clinopyroxene pixels in A are plotted with the same colors as in A. (For interpretation of the references to color in this figure legend, the reader is referred to the web version of this article.)

Two selection functions, namely 'identify pixels' and 'multi-groups', may be used to select ranges of composition (rectangles) in the diagrams, as well as to identify the selected pixels on the corresponding map (Figs. 4 and 5c) and to calculate modal abundances.

Several functions may be used to create masks from user-defined chemical groups within a phase. These masks are either built from manual selections (with the tools "identify pixel" and "multi-groups") or automatically using a *K-means* clustering approach. The mask variable can be exported into ASCII format (*.txt file) and used in the *Quanti* stage to export the average oxide composition corresponding to a selection of pixels (dashed arrows in Fig. 2).

2.4. Other functions

All the results can be saved and previously saved projects can be loaded at any time using the functions 'save', 'save as' and 'load'. The save functions store the data in a *MATLAB*© formatted binary file MAT-file (with .mat extension).

Functions in the 'figure' window are dedicated to the management of the color bar such as setting the minimum and maximum values, the auto and reset buttons, and the phase separator button (PhaseSep in Fig. 1). The user can also export the main figure in usual image formats.

Functions in the 'sampling' window are used to select a subset of the data into the main displayed image. These functions are available for any image (X-ray raw measurement, map of oxide compositions, structural formulae, equilibrium conditions maps). The selected data may be individual pixels, arrays or areas of pixels. This tool can be used for example to draw the composition variations of a mineral grain along a transect.

3. Tests and evaluation

Generating structural formulae and *P–T* maps from microprobe analysis is of interest for petrology and geodynamics studies. In this section, we present an example of the use of *XMapTools* on a metamorphic rock sample. Compositional maps were acquired on an eclogite sample from the Stak area, a high pressure (HP) continental massifs in NW Himalaya (Guillot et al., 2008; Riel et al., 2008; Lanari et al., 2013). This sample contains a well-preserved eclogitic assemblage consisting of garnet and omphacite, which formed during continental subduction. Omphacite was subsequently retrogressed to a Na-poorer clinopyroxene + plagioclase + amphibole symplectite. The final metamorphic event is recorded in the sample as a foliation comprising large crystals of amphibole developed as a result of deformation and syntectonic hydration under mid-upper crustal conditions (Lanari et al., 2013).

3.1. Data acquisition

An area of 0.348 mm^2 (520 μm × 670 μm) located in a symplectite zone and containing garnet, clinopyroxene, amphibole, plagioclase, Ti- and Fe-oxides was mapped at the Institute of Earth and Environmental Science, University of Potsdam, using a *JEOL* JXA-8200 EMPA. Mapping conditions were 15 keV accelerating voltage and 100 nA beam current, beam diameter smaller than 1 μm, 200 ms dwell time and 1 μm step size (i.e. pixel size). X-ray intensities for Si, Ti, Al, Fe, Mg, Mn, Ca, Na and K were measured in two passes.

3.2. Classification

An image of the mineral phases created using the 'mask creating function' (see §2.1) is shown in Fig. 6a. The two methods for the mask creating function (classical and normalized) were tested and lead to similar estimates of the mineral modal proportions except for garnet (Table 4). The difference for garnet is due to the erroneous allocation of the contour pixels around amphibole to the garnet mask when using the classical approach. This artefact may be corrected by creating an additional mask corresponding to the borders of the mineral or by using the normalized method. Additional differences between the 'normalized' and 'classical' approaches are shown in Fig. 6b for a part of the map (dashed square in Fig. 6a). For instance, zone 1 in Fig. 6b shows that omphacite is identified in the core of clinopyroxene using the 'normalized' method only. This is due to the normalization procedure and originates from the small chemical differences between omphacite and clinopyroxene in their Na- and Mg-contents. These

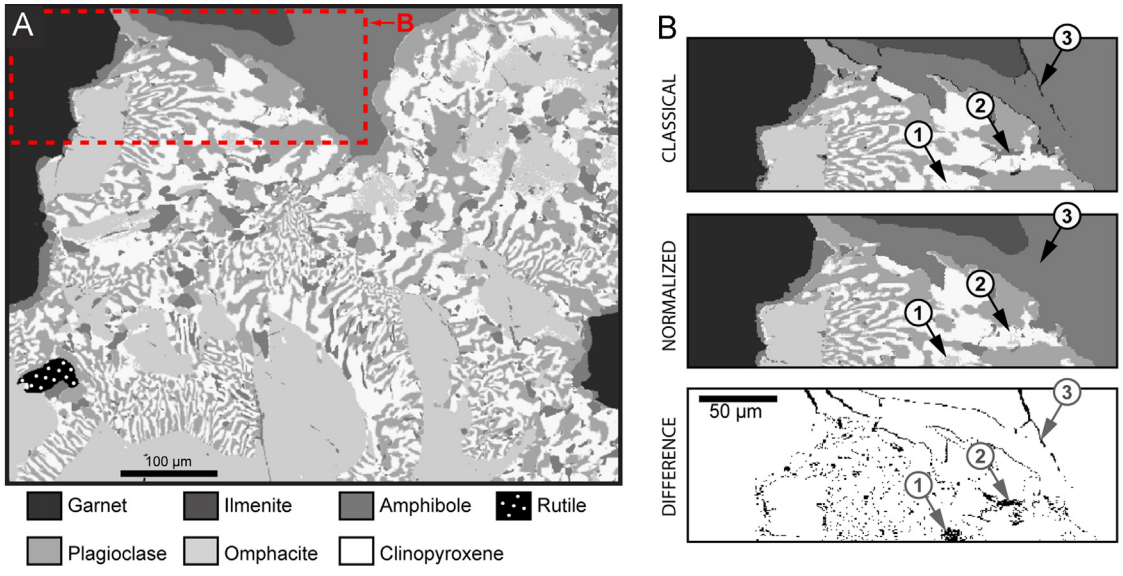

Fig. 6. Phase masks for the "eclogite" sample (A) computed using the 'normalized' method (see text). The part used to compare the two available methods is marked using a dashed rectangle. (B) Comparison between the "classical" and "normalized" methods with a difference image in which black pixels are the pixels not allocated to the same groups with both methods.

Table 4
Phase proportions (surface %) estimated with *XMapTools* using the available methods 'normalized' and 'classical'. The difference in percentage is an absolute difference.

	Normalized	Classical	Difference (%)
Ti-oxide	0.43	0.43	0
Garnet	7.00	7.70	9.09
Fe-oxide	1.10	1.13	2.65
Amphibole	13.20	12.77	3.37
Plagioclase	21.26	21.52	1.21
Omphacite	30.97	29.88	3.65
Cpx	26.04	26.57	1.99

Table 5
Uncertainties resulting from EPMA acquisition on raw data and error-propagation using Monte-Carlo techniques on quantified data and structural formulae for clinopyroxene. The precision at 2σ-level on raw data (in %) was estimated using the Eq. (1) on the average intensity of all the pixels of clinopyroxene. This uncertainty was propagated on the quantification process using a Monte-Carlo simulation with $n=100{,}000$ analyses. The uncertainty was similarly propagated on the structural formulae calculation process, including atom-site distribution.

Raw data			**Quantified data**		
Element	Mean intensity	Precision (% at 2σ)	Oxide	Composition	Error (2σ)
Si	11,086	1.8	SiO_2	54.72	0.99
Ti	93	20	TiO_2	0.18	0.04
Al	2529	4.0	Al_2O_3	9.69	0.38
Fe	631	8.0	FeO	4.53	0.36
Mg	1381	5.1	MgO	10.21	0.51
Ca	6486	2.4	CaO	16.38	0.39
Na	470	9.2	Na_2O	4.05	0.38
K	127	17	K_2O	0.02	0.01
			Structural formula		
				Composition	Error (2σ)
			Si_{T1}	1.96	0.02
			Al_{T1}	0.04	0.02
			Al_{M1}	0.37	0.02
			Mg_{M1}	0.55	0.03
			Fe_{M1}	0.13	0.01
			Ca_{M2}	0.62	0.02
			Na_{M2}	0.28	0.03
			XMg	0.80	0.01
			XFe	0.20	0.01
			X_{jd}	0.28	0.03
			X_{di}	0.54	0.03
			X_{hed}	0.14	0.01
			X_{cats}	0.02	0.01

differences are not detected with the 'classical' method, which allocates more pixels to the clinopyroxene mask. The other examples (2 and 3 in Fig. 6) show that in some cases, the opposite effect is observed when variations occur in only one highly concentrated element, keeping effects of the variations in low-concentrated elements to a minimum. From this, we conclude that the two methods should be tested and we recommend to check the difference between the two results and to compute different mask-files with different number of phases (including the fractures and/or mineral boundaries) (Table 5).

3.3. Test of the standardization

Analytical standardization of the X-ray images was performed using the 'standardization function' (see Section 2.1.2) with the 'Auto (median approach)' method. Calibration curves (graphical representation in Fig. 3) were calculated for clinopyroxene, garnet, amphibole and plagioclase.

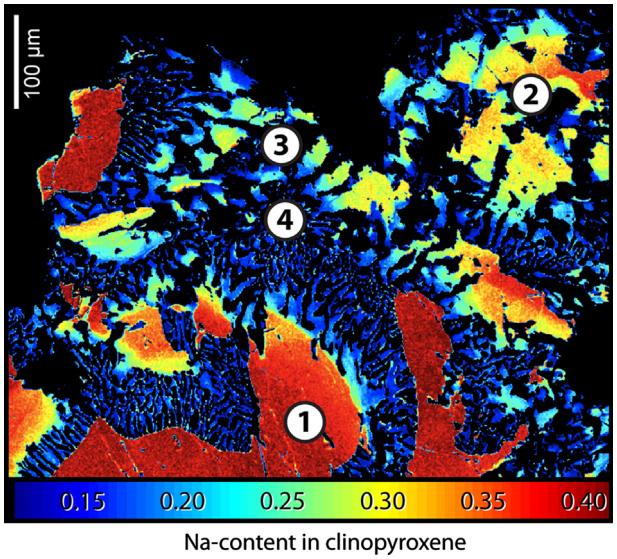

Fig. 7. Na-content of clinopyroxene (including omphacite). The different stages of crystallization (labeled 1–4) are discussed in the text.

The quality and accuracy of the standardization can be investigated using the function 'Test of standardization'. This function plots the composition difference between point analyses and the standardized composition on the same location on the maps. As an example, the results for the standardization of garnet are reported in Fig. 8, which shows that the pixel compositions derived from the standardized maps are in good agreement, within analytical uncertainties, with the corresponding point analyses for elements showing homogeneous compositions such as SiO_2, Al_2O_3, FeO (Fig. 8a, b and c) and heterogeneous compositions due to zoning such as CaO, MgO and MnO (Fig. 8d, e and f). In contrast, the point analyses of low concentration elements TiO_2 and K_2O show trends not recorded in the standardized maps (Fig. 8g and h), indicating that the concentrations of TiO_2 and K_2O mapped in garnet are not reliable, because they are close to the detection limits for the used mapping analytical conditions.

3.4. Structural formulae and chemical study

Clinopyroxene structural formulae were calculated on a 6 oxygen-basis by distributing elements on tetrahedral (T1) and octahedral (M1, M2) sites. End-members proportions of jadeite, diopside, hedenbergite, acmite and Ca-tschermak (Table 1) were estimated according to the atom site allocation model of Spear (1995) and Warren and Waters (2006). The amphiboles structural formulae were calculated on a 23 oxygen-basis and elements were distributed on tetrahedral (T1, T2), octahedral (M2, M13, M4), and 10 to 12-fold coordinated (A) sites. End-members proportions of glaucophane, tremolite, tschermakite, pargasite, cumingtonite (Table 1) were calculated according to the atom site allocation model of Dale et al. (2000; 2005). Structural formulae for garnet and plagioclase were respectively calculated on a 12 and 8 oxygen-basis following classical atom-site allocation models (Table 1). Structural formulae maps highlight the relationship between atom-site composition and microstructures. The two chemical modules *Chem2D* and *Triplot3D* were used to investigate the variations of clinopyroxene structural formulae (i.e. varying end-member proportions). In Fig. 4a, Na-rich clinopyroxene compositions were selected (red dots) using the 'identify pixel' tool (Section 2.3) in the Na vs. Mg diagram. The pixels belonging to the selected composition range

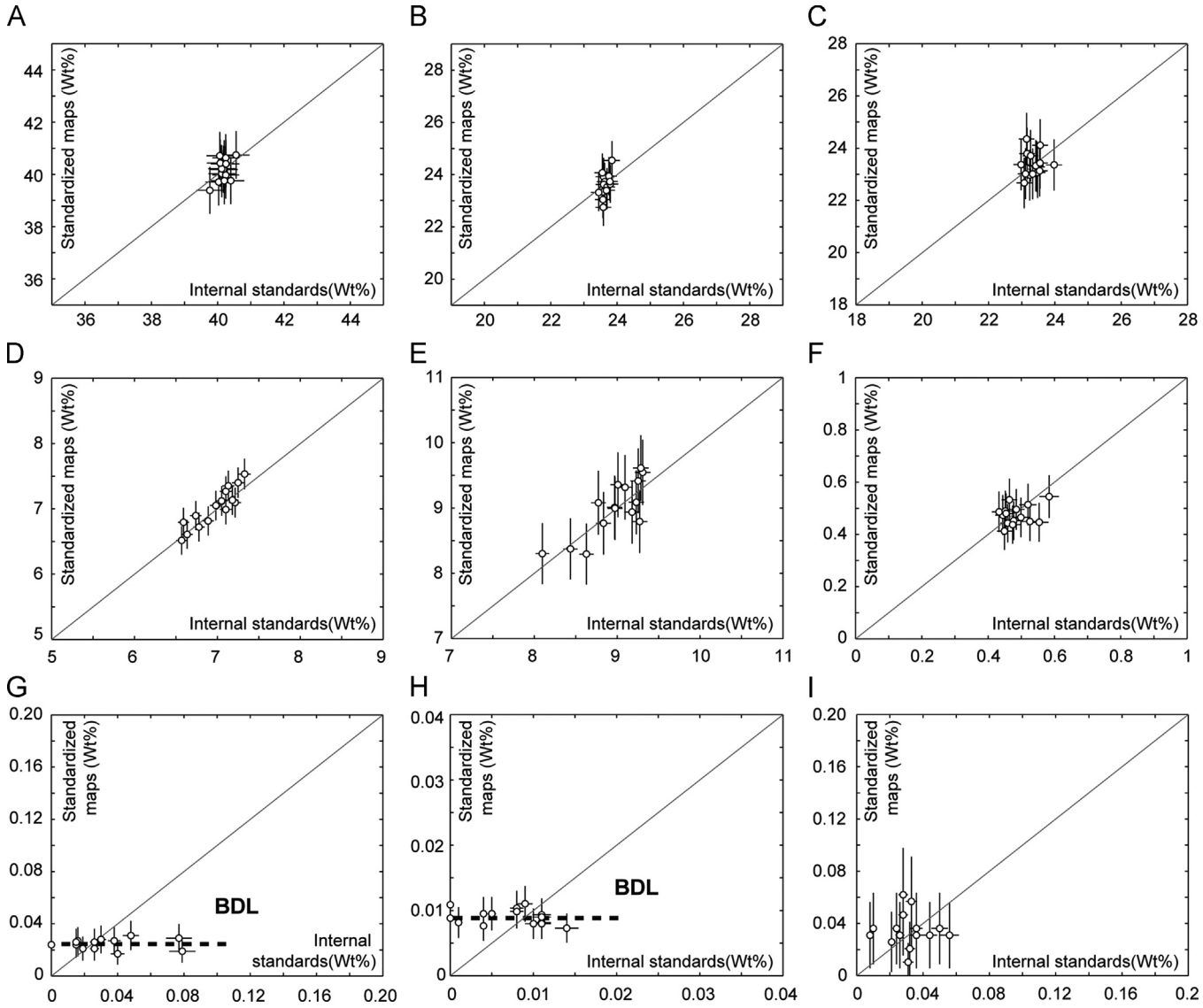

Fig. 8. Diagrams showing the difference between point analyses composition (standard) and the standardized composition on the same location on the X-ray maps for garnet and different elements. (A) SiO_2, (B) Al_2O_3, (C) FeO, (D) CaO, (E) MgO, (F) MnO, (G) TiO_2, (H) K_2O, (I) Na_2O. *BDL*: below detection limit.

are plotted in red on the map (Fig. 4c). These Na-rich clinopyroxene compositions are omphacitic and make up to ~25% of the total clinopyroxene pixels. Then, clinopyroxene compositions were divided into three groups using the 'multi-groups' tool within the jadeite-diopside-hedenbergite ternary diagram (groups 1, 2 and 3 in Fig. 5a). The pixels belonging to the three composition ranges are plotted on the map with corresponding colors (Fig. 5c). The clinopyroxene compositions into the symplectite have lower Na contents, corresponding to lower jadeite contents. Clinopyroxene-amphibole–plagioclase symplectites are known to nucleate on grain boundaries between two omphacite grains and to grow into the grain on one side, when the rock is sufficiently out of equilibrium to nucleate the product (Joanny et al., 1991; Waters, 2002; 2003). In the mapped area (Fig. 7), Na-rich clinopyroxene previously identified as omphacite shows high Na contents (up to 0.4 p.f.u, zone 1 in Fig. 7). This primary omphacite (width >100 μm) is destabilized into a first symplectite containing Na-poorer clinopyroxene, plagioclase and amphibole. Clinopyroxene in this first symplectite (zone 2 in Fig. 7) crystallizes as broad lamellae (30–40 μm width) preserving the original shape of omphacite, but with a lower Na-content (0.35 to 0.28 p.f.u.) than the original omphacite grains. A second symplectite with the same minerals is observed in zone 3 of Fig. 7, which shows smaller-size clinopyroxene lamellae (10–20 μm width) and Na-content (0.28 to 0.18 p.f.u.). Clinopyroxene lamellae are even smaller in the last symplectite (width <10 μm) and also have lower Na-content (<15 p.f.u.).

3.5. Precision and resolution

In the previous section, maps of structural formulae highlight variations in the clinopyroxene composition according to the symplectite microstructures. Na-content in clinopyroxene decreases with decreasing size of the symplectite (i.e. with time). The clinopyroxene solid solution includes jadeite while diopside hedenbergite and Ca-tschermak are calcic end-members. As the multiplicity of the M2 site is one and $XFe^{3+}=0$ (corresponding to $X_{acmite}=0$), the jadeite proportion is equal to the Na-content in clinopyroxene. Estimating the uncertainties associated with the compositional values of the structural formulae is needed before discussing the implications linked to the chemical zoning.

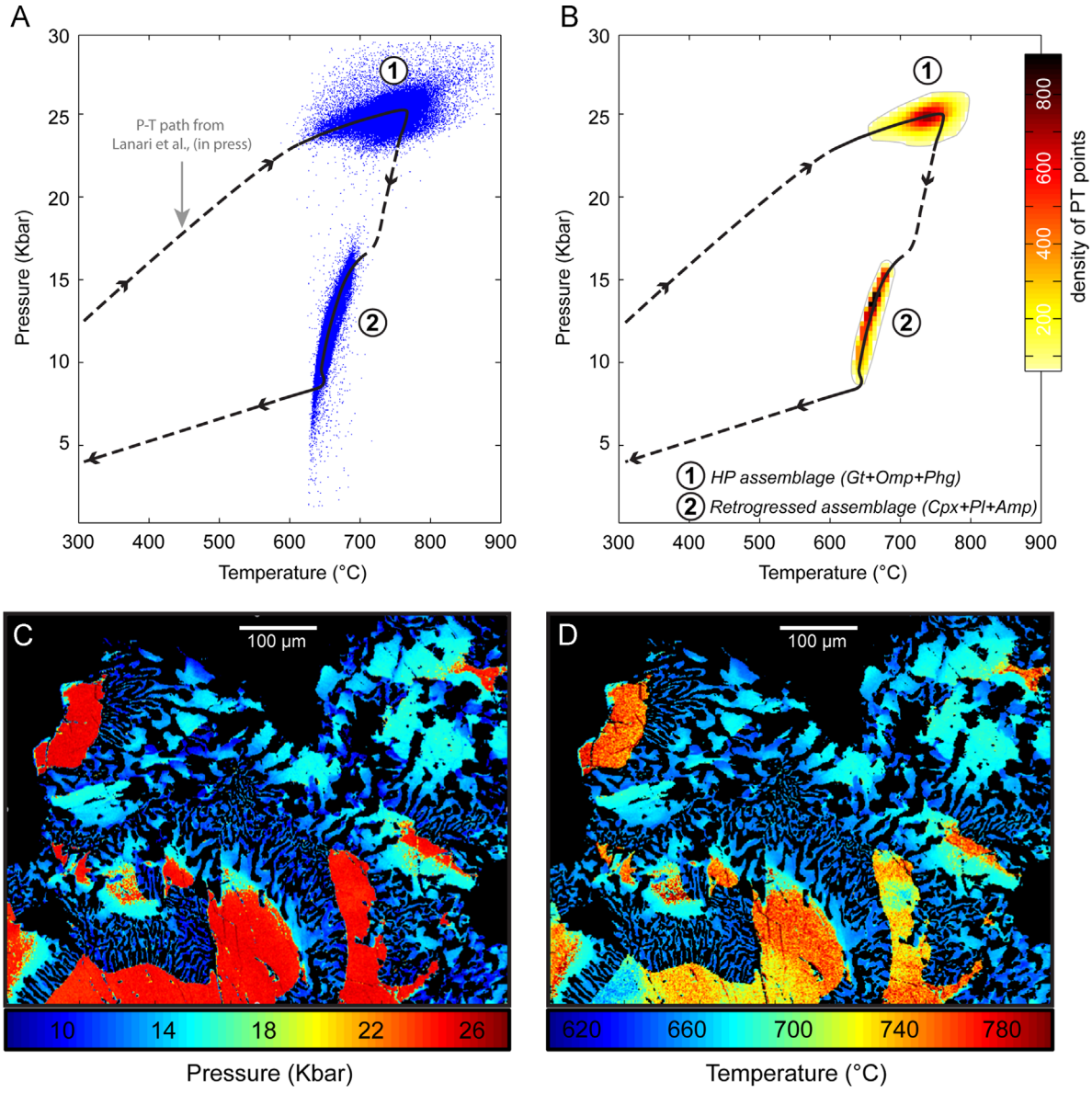

Fig. 9. *P–T* path and *P–T* maps of the Stak sample estimated from the compositions of clinopyroxene (see text for details). The interpreted *P–T* path is from Lanari et al. (2013).

The precision of the electron microprobe measurement with our experimental protocol can be estimated using a Poisson law (De Andrade et al., 2006):

$$p = \frac{2}{\sqrt{n}} \quad (1)$$

with p the precision (in % at 2σ), and n the number of recorded counts. The mean intensities and precision measurements for each element (Si, Ti, Al, Fe, Mg, Ca, Na, K) of clinopyroxene pixels are listed in Table 5. The precision measurements range from 1.8% for Si to 20% for Ti. Uncertainties in the structural formula originating from analytical errors were estimated using a Monte-Carlo simulation where a total of 100,000 random clinopyroxene compositions were computed with a normal distribution around the mean intensity compositions (Table 5) within 2σ of the measured precisions. The standardization procedure was carried out for all the compositions using the calibration curves estimated above. The average oxide concentrations structural formulae and the associated standard deviations are listed in Table 5. The average Na-content is estimated at 0.28 ± 0.03 p.f.u., which indicates that the compositional variations identified above (ranging from 0.41 to 0.13) are significant. It is emphasized that the uncertainties reported here are valid for the present EPMA settings and range of clinopyroxene composition, and can be decreased by increasing the dwell time.

3.6. Combined P and T functions: P–T maps of Cpx

P–T maps were built using combined *P* and *T* functions available in *XMapTools* (description in Section 2.2.2 and list in Table 3). At the thin section scale, two assemblages involving clinopyroxene are in equilibrium: the HP assemblage made of garnet, omphacite and phengite (as inclusions in garnet, not present in the mapped area) and the retrogressed assemblage represented by the clinopyroxene-plagioclase-amphibole symplectite. These two parageneses were treated separately.

For the HP assemblage, *P–T* conditions for clinopyroxene pixels were estimated using the *XMapTools* function 'Cpx-P-T Rav (Omp-Gar-Phg)'. *P* was estimated using the garnet, omphacite and phengite geobarometer of Waters and Martin (1993) and Waters (1996). *T* was estimated using the garnet and omphacite geothermometer of Ravna

(2000a). The function estimates first T_1 at a given P (P_{input}), and recalculates T_{n+1} and P_{n+1} until convergence (respectively 5 °C and 0.1 kbar) between T_n and T_{n+1} and P_n and P_{n+1}. As the compositions of garnet show a slight zoning (Alm_{48} Prp_{32-33} Grs_{17-19} Sps_1), two average garnet compositions were defined, one for the core and one for the rim (Lanari et al., 2013). In both groups, garnet compositions are homogeneous within errors. Each pixel of omphacite was assumed in equilibrium with one garnet average composition (core–core, rim–rim). Then, P–T estimates were calculated for all omphacite compositions.

For the symplectite, T was first estimated using the edenite–richterite calibration (Holland and Blundy, 1994) with the composition of amphibole pixels for a fixed composition of plagioclase (function 'Amp-T, Holland and Blundy 1994a'). Crystallization T for amphibole was found to vary from 680 ± 6 °C in contact with $Jd_{30\%}$ clinopyroxene to 640 ± 8 °C in contact with $Jd_{10\%}$ clinopyroxene. This relationship was used to calculate the T of clinopyroxene. P for clinopyroxene crystallization was subsequently calculated using the calibration of Waters (2003) for the equilibrium reaction: jad + trem = alb + ed.

About 165,000 P–T calculations (one for each Cpx pixel) have been obtained and the results have been plotted into binary diagrams (Fig. 9a and b) using the module Chem2D, and into P and T maps (Fig. 9c and d). The density P–T diagram option (Fig. 9b) plotted using the Chem2D module shows that the apparent deviation in P is composed of a small proportion of points (< 1%). In contrast, the density diagram shows a significant trend for T and P corresponding to the prograde evolution from 650 °C to 750 °C and from 24 kbar to 25 kbar. This increase in T and the slight increase of P along the prograde path is confirmed by the spatial distribution of the obtained T and P when plotted on a map: omphacite grains show high P at ~25 kbar, and are zoned in T from 650 °C in the old grain cores to 750 °C in the old grain rims. Clinopyroxene in the symplectite shows a different trend with a decrease of both P and T with the decreasing size of the intergrowths (Fig. 9). This interpretation on the preservation of P and T in symplectite during the exhumation is in good agreement with the reported high cooling rates (Guillot et al., 2009). This example typifies the importance of the mapping approach, which allows to test for relationships between P–T conditions and the textural information from metamorphic microstructures (Fig. 9).

4. Concluding remarks

This paper describes *XMapTools*, a MATLAB©-based GUI program to quantify raw X-ray electron microprobe data using internal standards, plot chemical diagrams and calculate P–T conditions of crystallization for metamorphic parageneses. The *XMapTools* program includes 15 user-friendly main functions for the different steps to the procedure, from the loading of the raw data to calculating P–T maps, and two external modules *Chem2D* and *TriPlot3D* with independent graphical user interfaces to plot chemical diagrams. Beside the treatment of compositional maps, *XMapTools* offers the possibility of estimating thermobarometric conditions, which can be linked to the observed deformation features. For the study of metamorphic and magmatic rocks, a set of external functions specific to geothermobarometry is also included. This set comprises a range of structural formulae functions for usual rock-forming silicate minerals as well as empirical and semi-empirical geothermobarometers from the literature. Application of *XMapTools* to an eclogite sample shows that the accuracy of the mapped minerals composition is good enough to discuss the compositional–structural–P–T relationships based from Na distribution in clinopyroxene. A strong link between metamorphic textures and composition has been found, and the retrieved P–T information gives a detailed reconstruction of the metamorphic history of the sample.

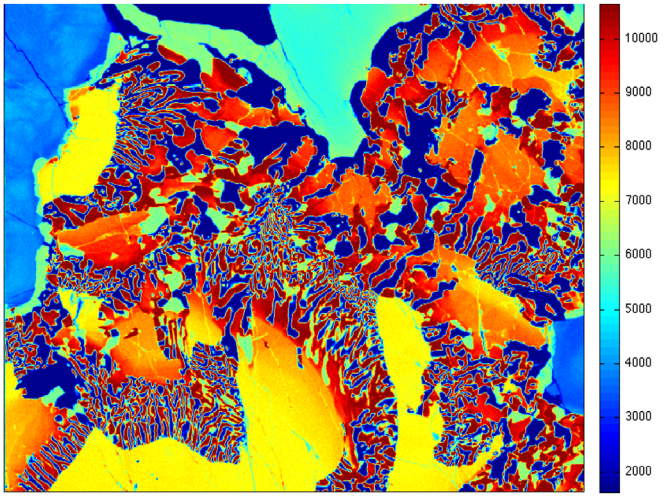

Fig. A1. Ca.txt chemical image (this file is available in Appendix A) for the high-pressure Himalayan eclogite sample from the Stak massif in northern Pakistan displayed using XMapTools (unit number of recorded counts, auto-contrast)..

A more detailed thermobarometric study can be made using independent programs such as e.g. Theriak-Domino (de Capitani and Petrakakis, 2010) or Tweeq (Berman, 2007) with the whole range of mineral compositions derived from *XMapTools*, which can be easily exported to the required formats. Moreover, an interesting feature of *XMapTools* is the possibility to calculating local bulk rock compositions from selected parts of the 2D maps. Such compositions can be used to calculate the stable mineral assemblages, compositions and abundance by free energy minimizing (e.g. Powell, 2008), and to compare them with the observed features. This approach, illustrated in Lanari et al. (2013) for the example discussed in the present contribution, can provide valuable information on the degree of achievement of thermodynamic equilibrium, the link between deformation and reequilibration, and possibly the extend of mass transfer controlled by deformation. Future release of *XMapTools* will incorporate energy minimizing and multi-equilibrium modules to facilitate advanced thermobarometric studies.

Acknowledgments

Authors acknowledge A. Pourteau for his help with the EPMA analyses, N. Riel, C. Martin, M. Burn, C. Loury, F. Guillot, B. Gardonio, F. Bernier, M. Engi, M. Muñoz, K. Malamoud, A. Robert, J. de Sigoyer, P. Agard and S. Guillot for help, comments, data and/or collaborations in order to test the different versions of *XMapTools*. Authors thank G. Ortolano, D. Waters and one anonymous reviewers for constructive comments and Jef Caers for editorial handling. This work was supported by the French ANR project "*ERD-Alps*".

Appendix A. Supporting information

Supplementary data associated with this article can be found in the online version at http://dx.doi.org/10.1016/j.cageo.2013.08.010.

References

Ai, Y., 1994. A revision of the garnet–clinopyroxene Fe^{2+}–Mg exchange geothermometer. Contributions to Mineralogy and Petrology 115 (4), 467–473.

Anderson, J.L., Smith, D.R., 1995. The effects of temperature and f_{O2} on the Al-in-hornblende barometer. American Mineralogist 80, 549–559.
Bence, A.E., Albee, A.E., 1968. Empirical correction factors for the electron microanalysis of silicates and oxides. Journal of Geology 76, 382–403.
Berman, R.G., 1991. Thermobarometry using multi-equilibrium calculations: a new technique, with petrological applications. Canadian Mineralogist 29, 833–855.
Berman, R.G., 2007. *WinTWQ* (version 2.3) a software package for performing internally-consistent thermobarometric calculations. Geological Survey of Canada, 41.
Blundy, J.D., Holland, T.J.B., 1990. Calcic amphibole equilibria and a new amphibole-plagioclase geothermometer. Contributions to Mineralogy and Petrology 104, 208–224.
Bonnet, N., 1998. Multivariate statistical methods for the analysis of microscope image series: applications in material science. Journal of Microscopy 190, 2–18.
Castaing, R., 1951. Application des sondes electronique a une methode d'analyse ponctuelle chimique et cristallographique. Université de Paris (publication ONERA), Paris.
Cathelineau, M., 1988. Cation site occupancy in chlorites and illites as function of temperature. Clay Minerals 23, 471–485.
Cathelineau, M., Nieva, D., 1985. A chlorite solid solution geothermometer the Los Azufres (Mexico) geothermal system. Contributions to Mineralogy and Petrology 91, 235–244.
Clarke, G.L., Daczko, N.R., Nockolds, C., 2001. A method for applying matrix corrections to X-ray intensity maps using the Bence–Albee algorithm and Matlab. Journal of Metamorphic Geology 19, 635–644.
Coggon, R., Holland, T., 2002. Mixing properties of phengitic micas and revised garnet-phengite thermobarometers. Journal of Metamorphic Geology 20, 683–696.
Cossio, R., Borghi, A., Ruffini, R., 2002. Quantitative modal determination of geological samples based on X-ray multielemental map acquisition. Microscopy and Microanalysis 8, 139–149.
Cosslett, V.E., Duncumb, P., 1956. Microanalysis by a flying-spot X-ray method. Nature 177, 1172–1173.
Creighton, S., 2009. A semi-empirical manganese-in-garnet single crystal thermometer. Lithos 112, 177–182.
Dahl, P.S., 1980. The thermal-compositional dependence of Fe^{2+}–Mg distributions between coexisting garnet and pyroxene: applications to geothermometry. American Mineralogist 65 (85), 866.
Dale, J., Holland, T., Powell, R., 2000. Hornblende–garnet–plagioclase thermobarometry: a natural assemblage calibration of the thermodynamics of hornblende. Contributions to Mineralogy and Petrology 140, 353–362.
Dale, J., Powell, R., White, R., Elmer, F., Holland, J., 2005. A thermodynamic model for Ca–Na clinoamphiboles in Na_2O–CaO–FeO–MgO–Al_2O_3–SiO_2–H_2O–O for petrological calculations. Journal of Metamorphic Geology 23, 771–791.
De Andrade, V., Vidal, O., Lewin, E., O'Brien, P., Agard, P., 2006. Quantification of electron microprobe compositional maps of rock thin sections: an optimized method and examples. Journal of Metamorphic Geology 24, 655–668.
de Capitani, C., Petrakakis, K., 2010. The computation of equilibrium assemblage diagrams with Theriak/Domino software. American Mineralogist 95, 1006–1016.
Dickenson, M., Hewitt, D., 1986. A garnet–chlorite geothermometer. Geological Society of America Abstracts 18, 584.
Dubacq, B., Vidal, O., Andrade, V., 2010. Dehydration of dioctahedral aluminous phyllosilicates: thermodynamic modelling and implications for thermobarometric estimates. Contributions to Mineralogy and Petrology 159, 159–174.
Ellis, D., Green, D., 1979. An experimental study of the effect of Ca upon garnet–clinopyroxene Fe–Mg exchange equilibria. Contributions to Mineralogy and Petrology 71, 13–22.
Fiannacca, P., Lo, Po, D., Ortolano, G., Cirrincione, R., Pezzino, A., 2012. Thermodynamic modeling assisted by multivariate statistical image analysis as a tool for unraveling metamorphic *P*–T–s evolution: an example from ilmenite–garnet-bearing metapelite of the Peloritani Mountains, Southern Italy. Mineralogy and Petrology 106, 151–171.
Friel, J.J., Lyman, 2006. X-ray mapping in electron-beam instruments. Microscopy and Microanalysis 12, 2–25.
Ganguly, J., 1979. Garnet and clinopyroxene solid solutions, and geothermometry based on Fe–Mg distribution coefficient. Geochimica et Cosmochimica Acta 43 (7), 1021–1029.
Ganne, J., De Andrade, V., Weinberg, R.F., Vidal, O., Dubacq, B., Kagambega, N., Naba, S., Baratoux, L., Jessell, M., Allibon, J., 2012. Modern-style plate subduction preserved in the Palaeoproterozoic West African craton. Nature Geoscience 5, 60–65.
Goldman, D., Albee, A., 1977. Correlation of Mg/Fe partitioning between garnet and biotite with O_{18}/O_{16} partitioning between quartz and magnetite. American Journal of Science 277, 750–761.
Graham, C., Powell, R., 1984. A garnet-hornblende geothermometer: calibration, testing, and application to the Pelona Schist, Southern California. Journal of Metamorphic Geology 2 (1), 13–31.
Grambling, J.A., 1990. Internally-consistent geothermometry and H_2O barometry in metamorphic rocks: the example garnet–chlorite–quartz. Contributions to Mineralogy and Petrology 105, 617–628.
Green, T., Hellman, P., 1982. Fe–Mg partitioning between coexisting garnet and phengite at high pressure, and comments on a garnet–phengite geothermometer. Lithos 15, 253–266.
Guillot, S., Riel, N., Hattori, K., Desgreniers, S., Rolland, Y., Van Melle, J., Latif, M., Kausar, A., Pêcher, A., 2008. New occurrence of eclogitic continental rocks in NW Himalaya: the Stak massif in northern Pakistan. Himalayan Journal of Sciences 5, 57–58.
Guillot, S., Hattori, K., Agard, P., Schwartz, S., Vidal, O., 2009. Exhumation processes in oceanic and continental subduction contexts: a review. In: Lallemand, S., Funiciello, F. (Eds.), Subduction Zone Dynamics. Springer-Verlag, Berlin Heidelberg, pp. 175–204, http://dx.doi.org/10.1007/978-3-540-87974-9.
Hammarstrom, J., Zen, E., 1986. Aluminum in hornblende; an empirical igneous geobarometer. American Mineralogist 71, 1297–1313.
Hillier, S., Velde, B., 1991. Octahedral occupancy and chemical composition of diagenetic (low-temperature) chlorites. Clay Minerals 26, 149.
Holdaway, M., Lee, S., 1977. Fe–Mg cordierite stability in high-grade pelitic rocks based on experimental theorical and natural observations. Contributions to Mineralogy and Petrology 63, 175–17198.
Holland, T., Baker, J., Powell, R., 1998. Mixing properties and activity-composition and relationships of chlorites in the system MgO–FeO–Al_2O_3–SiO_2–H_2O. European Journal of Mineralogy 10, 395–406.
Holland, T., Blundy, J., 1994. Non-ideal interactions in calcic amphiboles and their bearing on amphibole-plagioclase thermometry. Contributions to Mineralogy and Petrology 116, 433–447.
Holland, T., Powell, R., 1998. An internally consistent thermodynamic data set for phases of petrological interest. Journal of Metamorphic Geology 16, 309–343.
Holland, T., Powell, R., 2011. An improved and extended internally consistent thermodynamic dataset for phases of petrological interest, involving a new equation of state for solids. Journal of Metamorphic Geology 29, 333–383.
Hollister, L.S., Grissom, G., Peters, E., Stowell, H., Sisson, V., 1987. Confirmation of the empirical correlation of Al in hornblende with pressure of solidification of calc-alkaline plutons. American Mineralogist 72, 231.
Inoue, A., Meunier, A., Patrier-Mas, P., Rigault, C., Beaufort, D., Vieillard, P., 2009. Application of chemical geothermometry to low-temperature trioctahedral chlorites. Clays and Clay Minerals 57, 371–382.
Joanny, V., van Roermund, H., Lardeaux, J.M., 1991. The clinopyroxene/plagioclase sympelctite in retrograde eclogites: a potential geothermobarometer. Geologische Rundschau 80 (2), 303–320.
Johnson, M., Rutherford, M., 1989. Experimental calibration of the aluminum-in-hornblende geobarometer with application to Long Valley valdera (California) volcanic rocks. Geology 17, 837–841.
Jowett, E., 1991. Fitting iron and magnesium into the hydrothermal chlorite geothermometer: GAC/MAC/SEG. Presented at the Joint Annual Meeting, Toronto, May 27-29, 1991, Program with Abstracts.
Kawasaki, T., Nakano, N., Osanai, Y., 2011. Osumilite and a spinel+quartz association in garnet–sillimanite gneiss from Rundvågshetta, Lützow–Holm Complex, East Antarctica. Gondwana Research 19, 430–445.
Kohn, M.J., Spear, F., 2000. Retrograde net transfer reaction insurance for pressure-temperature estimates. Geology 28, 1127–1130.
Kranidiotis, P., MacLean, W., 1987. Systematics of chlorite alteration at the Phelps Dodge massive sulfide deposit, Matagami, Quebec. Economic Geology and the Bulletin of Society of Economic Geologists 82, 1898–1911.
Krogh, E.J., Råheim, A., 1978. Temperature and pressure dependence of Fe–Mg partitioning between garnet and phengite, with particular reference to eclogites. Contributions to Mineralogy and Petrology 66, 75–80.
Krogh, E.J., 1988. The garnet–clinopyroxene Fe–Mg geothermometer a reinterpretation of existing experimental data. Contributions to Mineralogy and Petrology 99 (1), 44–48.
Lanari, P., Guillot, S., Schwartz, S., Vidal, O., Tricart, P., Riel, N., Beyssac, O., 2012. Diachronous evolution of the alpine continental subduction wedge: evidence from *P*–*T* estimates in the Briançonnais Zone houillère (France–Western Alps). Journal of Geodynamics 56-57, 39–54.
Lanari, P., Riel, N., Guillot, S., Vidal, O., Schwartz, S., Pêcher, A., Hattori, K., 2013. Deciphering high-pressure metamorphism in collisional context using microprobe-mapping methods: application to the Stak eclogitic massif (NW Himalaya). Geology 41, 111–114.
Launeau, P., Cruden, A.R., Bouchez, J.L., 1994. Mineral recognition in digital images of rocks: a new approach using multichannel classification. Canadian Mineralogist 32, 919–933.
Martin, C., Debaille, V., Lanari, P., Goderist, S., Vanhaecke, F., Vidal, O., Claeys, P., 2013. REE and Hf distribution among mineral phases in the CV-CK clan: a way to explain present-day Hf isotopic variations in chondrites. Geochimica and Cosmochimica Acta 120, 495-513.
Massone, H., Schreyer, W., 1987. Phengite geobarometry based on the limiting assemblage with K-feldspar, phlogopite and quartz. Contributions to Mineralogy and Petrology 96, 212–224.
Mori, T., Green, D., 1978. Laboratory duplication of phase equilibria observed in natural garnet lherzolites. Journal of Geology 86, 83–97.
Muñoz, M., De Andrade, V., Vidal, O., Lewin, E., Pascarelli, S., Susini, J., 2006. Redox and speciation micromapping using dispersive X-ray absorption spectroscopy: application to iron in chlorite mineral of a metamorphic rock thin section. Geochemistry, Geophysics, Geosystems 7 (11), 1–10.
Mysen, B., Heier, K., 1972. Petrogenesis of eclogites in high grade metamorphic gneisses, exemplified by the Hareidland eclogite, western Norway. Contributions to Mineralogy and Petrology 36 (1), 73–94.
Pattison, D.R.M., Newton, R.C., 1989. Reversed experimental calibration of the garnet–clinopyroxene Fe–Mg exchange thermometer. Contributions to Mineralogy and Petrology 101, 87–103.
Parra, T., Vidal, O., Agard, P., 2002. A thermodynamic model for Fe–Mg dioctahedral K white micas using data from phase-equilibrium experiments and natural pelitic assemblages. Contributions to Mineralogy and Petrology 143, 706–732.

Perchuk, L., Aranovich, L.Y., Podlesskii, K., Lavrent'eva, I., Gerasimov, V., Fed'kin, V., Kitsul, V., Karsakov, L., Bernikov, N., 1985. Precambrian granulites of the Aldan shield, eastern Siberia, USSR. Journal of Metamorphic Geology 3, 265–310.
Plunder, A., Agard, P., Dubacq, B., Chopin, C., Bellanger, M., 2012. How continuous and precise is the record of *P–T* paths? Insights from combined thermobarometry and thermodynamic modelling into subduction dynamics (Schistes Lustrés, W. Alps). Journal of Metamorphic Geology 30, 323–346.
Powell, R., 1985. Regression diagnostics and robust regression in geothermometer/geobarometer calibration: the garnet–clinopyroxene geothermometer revisited. Journal of Metamorphic Geology 3, 231–243.
Powell, R., 2008. On thermobarometry. Journal of Metamorphic Geology 26, 155–179.
Pourteau, L., Sudo, M., Candan, O., Lanari, P., Vidal, O., Oberhänsli, R., 2013. Neotethys closure history of Anatolia: insights from 40Ar–39Ar geochronology and *P–T* estimation in high pressure metasedimentary rocks. Journal of Metamorphic Geology 31 (6), 585–606.
Prêt, D., Sammartino, S., Beaufort, D., Meunier, A., Fialin, M., Michot, L.J., 2010. A new method for quantitative petrography based on image processing of chemical element maps: Part I. Mineral mapping applied to compacted bentonites. American Mineralogist 95, 1379–1388.
Råheim, A., Green, D.H., 1974. Experimental determination of the temperature and pressure dependence of the Fe–Mg partition coefficient for coexisting garnet and clinopyroxene. Contributions to Mineralogy and Petrology 48, 179–203.
Ravna, E.K., 2000a. The garnet–clinopyroxene Fe^{2+}–Mg geothermometer: an updated calibration. Journal of Metamorphic Geology 18, 211–219.
Ravna, E.K., 2000b. Distribution of Fe^{2+} and Mg between coexisting garnet and hornblende in synthetic and natural systems: an empirical calibration of the garnet–hornblende Fe–Mg geothermometer. Lithos 53, 265–277.
Reed, S.J.B., 2005. Electron Microprobe Analysis and Scanning Electron Microscopy in Geology, 2nd edition Cambridge University Press, Cambridge.
Riel, N., Hattori, K., Guillot, S., Rayner, N., Davis, N., Latif, M., Kausar, M., 2008. SHRIMP zircon ages of eclogites in the Stak massif, northern Pakistan. Himalayan Journal of Sciences 5, 119–120.
Saporta, G., 1990. Probabilités, analyse des données et statistique. Editions Technip, Paris.
Schmidt, M.W., 1992. Amphibole composition in tonalite as a function of pressure: an experimental calibration of the Al-in-hornblende barometer. Contributions to Mineralogy and Petrology 110, 304–310.
Seber, G., 1984. Multivariate Observations. John Wiley & Sons, Inc., Hoboken, NJ.
Sengupta, P., Dasgupta, S., Bhattacharya, P.K., Hariya, Y., 1989. Mixing behavior in quaternary garnet solid solution and an extended Ellis and Green garnet–clinopyroxene geothermometer. Contributions to Mineralogy and Petrology 103, 223–227.
Spath, H., 1985. Cluster Dissection and Analysis: Theory, FORTRAN Programs, Examples. Halsted Press, New York.
Spear, F., 1995. Metamorphic Phase Equilibria and Pressure–Temperature–Time Paths. Mineral Society of America, Washington.
Thompson, A., 1976. Mineral reactions in pelitic rocks: II. Calculation of some *P–T*–X (Fe–Mg) phase relations. American Journal of Science 276, 425–454.
Tinkham, D.K., Ghent, E.D., 2005. XRMapAnal: a program for analysis of quantitative X-ray maps. American Mineralogist 90, 737–744.
Vidal, O., Parra, T., 2000. Exhumation paths of high-pressure metapelites obtained from local equilibria for chlorite–phengite assemblages. Geological Journal 35, 139–161.
Vidal, O., Goffé, B., Bousquet, R., Parra, T., 1999. Calibration and testing of an empirical chloritoid–chlorite Mg–Fe exchange thermometer and thermodynamic data for daphnite. Journal of Metamorphic Geology 17, 25–39.
Vidal, O., Parra, T., Trotet, F., 2001. A thermodynamic model for Fe–Mg aluminous chlorite using data from phase equilibrium experiments and natural pelitic assemblages in the 100 to 600 °C, 1 to 25 kb range. American Journal of Science 301, 557.
Vidal, O., Parra, T., Vieillard, P., 2005. Thermodynamic properties of the Tschermak solid solution in Fe-chlorite: application to natural examples and possible role of oxidation. American Mineralogist 90, 347–358.
Vidal, O., De Andrade, V., Lewin, E., Munoz, M., Parra, T., Pascarelli, S., 2006. *P–T*-deformation-Fe^{3+}/Fe^{2+} mapping at the thin section scale and comparison with XANES mapping: application to a garnet-bearing metapelite from the Sambagawa metamorphic belt (Japan). Journal of Metamorphic Geology 24, 669–683.
Warren, C., Waters, D., 2006. Oxidized eclogites and garnet–blueschists from Oman: *P–T* path modelling in the NCFMASHO system. Journal of Metamorphic Geology 24, 1–20.
Waters, D., 1996. The Garnet–Cpx–Phengite barometer. Recommended calibration and calculation method. ⟨http://www.earth.ox.ac.uk/~davewa/research/eclogite/ecbarcal.html⟩ (updated 01.03.96).
Waters, D., 2002. Clinopyroxene–Amphibole–plagioclase symplectites in Norwegian eclogites: microstructures, chemistry and the exhumation *P–T* path. In: Proceedings of the Winter Conference of the Mineralogical Society, Derby.
Waters, D., 2003. *P–T* paths from Cpx–Hbl–Pl symplectites, updated 22 February 2003. ⟨http://www.earth.ox.ac.uk/~davewa/research/eclogites/symplectites.html⟩ (updated 22.02.03).
Waters, D., Martin, H., 1993. Geobarometry in phengite-bearing eclogites. Terra Nova 5, 410–411.
Yamato, P., Agard, P., Burov, E., Le Pourhiet, L., Jolivet, L., Tiberi, C., 2007. Burial and exhumation in a subduction wedge: mutual constraints from thermomechanical modeling and natural *P–T–t* data (Schistes Lustrés, western Alps). Journal of Geophysical Research 112, B07410.
Zack, T., Moraes, R., Kronz, A., 2004. Temperature dependence of Zr in rutile: empirical calibration of a rutile thermometer. Contributions to Mineralogy and Petrology 148, 471–488.
Zang, W., Fyfe, W., 1995. Chloritization of the hydrothermally altered bedrock at the Igarape Bahia gold deposit, Carajas, Brazil. Mineralium Deposita 30, 30–38.